Modeling temperature-dependent transport properties in dissipative particle dynamics: A top-down coarse-graining toward realistic dynamics at the mesoscale

Modeling temperature-dependent transport properties in dissipative particle dynamics: A top-down coarse-graining toward realistic dynamics at the mesoscale

N. Lauriello,[1, a)] M. Lísal,[2, 3] G. Boccardo,[1] D. Marchisio,[1] and A. Buffo[1]

[1)]*DISAT – Institute of Chemical Engineering, Politecnico di Torino, C.so Duca degli Abruzzi 24, Torino 10129, Italy*

[2)]*Research Group of Molecular and Mesoscopic Modelling, The Czech Academy of Sciences, Institute of Chemical Process Fundamentals, Rozvojová 135/1, Prague, Czech Republic*

[3)]*Department of Physics, Faculty of Science, Jan Evangelista Purkyně University in Ústí nad Labem, Pasteurova 3544/1, 400 96 Ústí n. Lab., Czech Republic*

(Dated: 30 May 2024)

Dissipative particle dynamics (DPD) is a widespread computational tool to simulate the behavior of soft matter and liquids in- and out-of-equilibrium. Although there are many applications where the effect of temperature is relevant, most of DPD studies have been carried out at a fixed system temperature. Therefore, this work investigates how to incorporate the effect of system temperature variation within the DPD model to capture realistic temperature-dependent system properties. In particular, this work focuses on the relationship between temperature and transport properties and therefore, an extended DPD model for transport properties prediction is employed. Transport properties, unlike the equilibrium properties, are often overlooked despite of their significant influence on the flow dynamics of non-isothermal mesoscopic systems. Moreover before simulating the response of the system induced by a temperature change, it is first important to estimate transport properties at a certain temperature. Thus here, the same fluid is simulated across different temperature conditions using isothermal DPD with the aim to identify a temperature-dependent parametrization methodology, capable to ensure the correctness of both equilibrium and dynamical properties. Liquid water is used as a model system for this analyses. This work proposes a temperature-dependent form of the extended DPD model where both conservative and non-conservative interaction parameters incorporate the variation of the temperature. The predictions provided by our simulations are in excellent agreement with experimental data.

[a)] Author to whom correspondence should be addressed: nunzia.lauriello@polito.it.

I. INTRODUCTION

Soft materials include polymeric solutions and melts, suspensions of colloidal particles, micellar solutions and liquid foams, and they are very common in food, personal care and pharmaceutical industries[1]. The rational design and performance optimization of such materials and equipment involved in their processing require the ability to predict their morphology and their properties on engineering length and time scales in a reasonable time. The design of these systems is challenged by the extensive experimental campaign required to estimate material properties, which are influenced by many variables such as composition and temperature. For example, it is not straightforward to theoretically predict the concomitant changes of morphology and material properties induced by temperature changes. On the other hand, approaches relying only on laboratory measurements are costly and time consuming[2].

The use of computational tools to carry out virtual experiments to screen or predict materials properties is an interesting alternative, as they typically allow to mimic different temperature conditions. Among the different computational tools available for estimating soft materials properties coarse-grain (CG) molecular dynamics (MD), a very well-known mesoscopic technique, can profitably be used, as it addresses the involved time and length scales. In fact, the computational model should describe the microstructures and morphologies that dictate the final soft materials properties.

Among the different mesoscopic methods, Dissipative Particle Dynamics (DPD) is one of the most successful CG MD techniques. It is employed to explore the behavior of soft matter systems over relevant time and length scales[3–6]. It operates at time and length scales larger than those of all-atom MD, allowing for the prediction of both equilibrium and dynamical properties[7,8]. The reason for this is that it is a CG MD model. Groups of atoms and molecules are treated as single entities called beads, interacting via a mesoscopic force field, made of conservative soft-repulsive and non-conservative interactions. DPD was introduced originally by Hoogerbrugge and Koelman[9] and later on developed by Español and Warren[10]. Due to its promising computational benefits and versatility, the DPD method has been further developed and in the past two decades has been successfully applied to a wide range of applications involving simple and complex systems[11,12].

However, there are still some gaps in the method which narrow its scope of application. For example, there are long standing ambiguities regarding the introduction of the system temperature variation into the model. Recently a growing and promising trend towards the modification of

the conventional DPD model, appropriate for the non-isothermal simulation of conservative interaction force fields, that are both density- and temperature-dependent, is slowly emerging[13–15]. In other cases, the temperature enters into the definition of the model only parametrically without modifying the conventional framework of the DPD model. Different approaches calculate the temperature effect on the DPD conservative repulsive parameters for both simple and complex fluids and successfully validate them against equilibrium properties[7,16,17]. Regardless of the approach followed, the application of a DPD model, which incorporates temperature-dependent conservative interactions, allows to describe accurately equilibrium properties when the temperature varies. However, it does not ensure the simultaneous correct prediction of transport properties. In fact, transport properties are strongly affected by non-conservative interactions, which have no effect on equilibrium properties such as thermodynamics and the system structure.

Most of DPD studies on transport properties were carried out without varying temperature, although transport properties usually vary strongly with the system temperature and the effect of temperature on the flow dynamics of non-isothermal mesoscopic systems is not negligible. Since the modification of the non-conservative interaction force field is not straightforward, the temperature effect is just introduced parametrically into non-conservative interactions in order to capture the effect of temperature. However, these studies employed the standard DPD thermostat which, relying on parallel dissipative forces acting in the radial direction only, cannot properly model liquid-like dynamics. Several studies claimed that it fails in the prediction of real fluids transport properties[18,19]. In fact, the contribution of shear dissipative forces, in the direction perpendicular to the interatomic axis, is important to ensure a correct description of transport properties. A different thermostat for DPD, a transverse DPD thermostat, is obtained by also describing the perpendicular damping[20]. Our previous studies demonstrate that a particular extension of the DPD model, based on a transverse thermostat, together with the modification of the weighting function for the dissipative and random (non-conservative) forces[19,21], allows to finely tune transport properties by calibrating non-conservative interaction parameters against convenient experimental transport properties.

This work proposes, for the first time, a temperature-dependent form of the extended DPD model, where both conservative and non-conservative interaction parameters incorporate the system temperature variation obtained by fitting experimental observables. The extended DPD model of this work is developed using the top-down CGing as its conservative and non-conservative interaction parameters are fitted to experimental observables of a real system.

Bottom-up CGings, which rely on atomistic simulations, also exist and a typical example includes multi-scale CGing (force matching)[22,23]. Here within the Mori-Zwanzig projection operator method[24,25], the CG equations of motion (EoM) can be uniquely determined by the underlying microscopic dynamics. They have a form of the generalized Langevin equation and describe the evolution of a subset of the degrees of freedom. Under Markovian approximation, the generalized Langevin equation can be reduced to DPD EoM with conservative, dissipative force and random forces whose expressions can be obtained directly from atomistic simulations.

In this work, instead, a top-down procedure is adopted for the parametrization of non-conservative interactions. This strategy does not require large molecular dynamics trajectories to inform the DPD model, reducing the computational effort. The objective is to enable the model to simulate a liquid across different temperatures, describing accurately not only equilibrium properties, but also transport properties at various temperatures. Isothermal simulations across different temperatures are carried out, since the estimation of transport properties at a given temperature is important before evaluating the dynamical behavior induced by thermal gradients. Moreover, transport properties are measured using an equilibrium approach. This is advantageous in self-assembled systems, since it allows the estimation of viscosity in equilibrium without altering their equilibrium self-assembled microstructures. In fact, before evaluating the rheological behavior of self-assembled systems related to the structural changes occurring under fluid motion or temperature change, it is important at first to estimate the viscosity of morphologies in equilibrium without perturbing them.

In particular, we selected liquid water as model system and used experimental data of transport properties[26,27] from 5°C to 90°C as target values to develop and validate the extended DPD model. Moreover, we also assessed the performance of the Shardlow-splitting-algorithm-based integration scheme (VV-SSA), which was proved to be superior to the standard velocity-Verlet for the evaluation of transport properties, to solve the isothermal extended DPD model EoM varying the system temperature. We employed the automated method (AMTP_DPD), presented in our previous work[21], to compute transport properties with controlled accuracy from DPD equilibrium simulations carried out across different temperatures. The application of the proposed model provides estimates for liquid water transport properties in excellent agreement with experimental data across the whole liquid temperatures range. In addition, we enabled the open source code LAMMPS[28] to evaluate numerically the conservative and non-conservative force contributions of the viscosity to investigate their relative weight and their behavior with respect to the system tem-

perature. This type of additional calculation allowed to make comparison with theoretical data available in the literature.

The outline of the article is as follows. Section II presents the DPD EoM of the extended DPD model, the time integration scheme and the method for the evaluation of the transport properties employed. Section III describes the computational details and illustrates the setup of the simulations carried out. Section IV presents the top-down methodology followed to develop a temperature-dependent form of the extended DPD model to reproduce correctly water transport properties across the whole temperature range. The results are presented and discussed in the context of a comparison with both experimental and theoretical expectations, leaving the conclusions in Section V.

II. DISSIPATIVE PARTICLE DYNAMICS: THE MODEL DETAILS

A. Governing equations, parametrization and reduced units

DPD is a particle-based mesoscopic simulation technique, where groups of atoms are projected into a statistically equivalent ensemble of structureless CG particles, the so-called beads, interacting via a mesoscopic force field. The DPD force field consists of variables in reduced units, the so-called DPD units. Typically in DPD, the mass of a single DPD bead, conservative cut-off radius and thermal energy are taken as, respectively, mass, time and energy units. Thus, other quantities such as the viscosity and diffusivity of the system are not defined explicitly but in terms of the DPD units. The time evolution of each bead can be calculated by the Newton second law as

$$\frac{d\boldsymbol{r}_i}{dt} = \boldsymbol{v}_i, \quad \frac{d\boldsymbol{v}_i}{dt} = \frac{\boldsymbol{f}_i}{m_i}, \tag{1}$$

with $i = 1,..,N$; $\boldsymbol{r}_i$ and $\boldsymbol{v}_i$ are the position and velocity of the bead i with mass m_i, respectively, and N is the number of DPD beads in the system. In the case of a DPD fluid, the force $\boldsymbol{f}_i$ acting on the $i-$th bead is the sum of three pairwise contributions:

$$\boldsymbol{f}_i = \sum_{j \neq i} (\boldsymbol{F}_{ij}^C + \boldsymbol{F}_{ij}^D + \boldsymbol{F}_{ij}^R). \tag{2}$$

In Eq. (2), the sum runs over the indices of beads contained in the closest vicinity of bead i within a certain cut-off radius r_c. The conservative contribution, $\boldsymbol{F}_{ij}^C$, is a soft-repulsive force acting

between a pair of beads i and j, and having the following functional form

$$\boldsymbol{F}_{ij}^{C} = \begin{cases} a_{ij}\left(1-\frac{r_{ij}}{r_c^C}\right)\hat{\boldsymbol{r}}_{ij}, & r_{ij} < r_c^C \\ 0, & r_{ij} > r_c^C \end{cases} \tag{3}$$

where a_{ij} denotes a maximum repulsion (a repulsive parameter) between beads i and j, $r_{ij} = |\boldsymbol{r}_{ij}| = |\boldsymbol{r}_i - \boldsymbol{r}_j|$ is the separation distance between a pair of beads, and $\hat{\boldsymbol{r}}_{ij} = \boldsymbol{r}_{ij}/r_{ij}$ is the unit vector of the bead-bead separation distance and r_c^C is the cut-off radius for the conservative interactions. Dissipative and random forces, $\boldsymbol{F}_{ij}^{D}$ and $\boldsymbol{F}_{ij}^{R}$, respectively, represent the the effect of viscosity slowing down the particles motion with respect to each other and of thermal/vibrational energy of the system. They act together as a thermostat. The random and dissipative forces are coupled via the fluctuation–dissipation theorem (FDT)[29], ensuring sampling from the appropriate probability distribution. In addition, DPD conserves the total momentum.

Expressions for the dissipative and random forces, and their parameters, as introduced by Groot and Warren in their seminal DPD work[7], yield unrealistically low values of the Schmidt number, $Sc \approx 1$, i.e., gas-like dynamics while realistic liquids exhibit Sc of $\mathcal{O}(10^2)$, e.g., $Sc \approx 400$ for ambient water. Several authors[18,19,21,30,31] demonstrated necessity to extend and generalize Groot-Warren's expressions for the non-conservative forces. It includes employing parallel and perpendicular contributions to the non-conservative forces, as suggested by Junghans et al.[20], and use of generalized weighting functions, i.e.,

$$\boldsymbol{F}_{ij}^{D} = -\gamma_{\parallel} w_{\parallel}^2(r_{ij})(\hat{\boldsymbol{r}}_{ij}\cdot\boldsymbol{v}_{ij})\hat{\boldsymbol{r}}_{ij} - \gamma_{\perp} w_{\perp}^2(r_{ij})(\boldsymbol{I}-\hat{\boldsymbol{r}}_{ij}\hat{\boldsymbol{r}}_{ij}^{T})\boldsymbol{v}_{ij}, \tag{4}$$

$$\boldsymbol{F}_{ij}^{R} = \sigma_{\parallel} w_{\parallel}(r_{ij})\frac{\xi_{ij}}{\sqrt{\Delta t}}\hat{\boldsymbol{r}}_{ij} + \sigma_{\perp} w_{\perp}(r_{ij})(\boldsymbol{I}-\hat{\boldsymbol{r}}_{ij}\hat{\boldsymbol{r}}_{ij}^{T})\frac{\boldsymbol{\xi}_{ij}}{\sqrt{\Delta t}}. \tag{5}$$

Here, $\gamma_{\parallel}$ and $\gamma_{\perp}$ are parallel and perpendicular dissipative coefficients, respectively, and analogously $\sigma_{\parallel}$ and $\sigma_{\perp}$ are parallel and perpendicular noise coefficients, $w_{\parallel}(r_{ij})$ and $w_{\perp}(r_{ij})$ are weighting functions for the parallel and perpendicular parts of $\boldsymbol{F}_{ij}^{D}$ and $\boldsymbol{F}_{ij}^{R}$, $\boldsymbol{v}_{ij} = \boldsymbol{v}_i - \boldsymbol{v}_j$, ξ_{ij} and $\boldsymbol{\xi}_{ij}$ are scalar and vector random numbers, respectively, with zero mean value and unit variance, $\boldsymbol{I}$ is the identity second-rank matrix and Δt is the simulation timestep. The dissipative and noise parameters satisfy the FDT

$$\sigma_{\alpha} = \sqrt{2k_B T\gamma_{\alpha}}, \quad \alpha \in \{\parallel, \perp\}, \tag{6}$$

where k_B denotes the Boltzmann constant and T is the system temperature.

The description of shear dissipation fills a significant deficiency of the standard DPD method that negatively affects the capability to predict transport properties of real liquids. The conventional DPD formulation includes only radial frictions while the microscopic generalized Langevin equation indicates the presence of non-central shear. To restore angular momentum conservation violated due to the presence of non-central shear forces, additional equations for torques and angular velocities of the particles need to be introduced[10,32]. The major drawback of this approach is the computational time, which is higher with respect to the standard or extended DPD due to the evaluation of the rotational damping contribution. However, the requirement on angular momentum conservation is particularly important when non-equilibrium simulations are used to measure the fluid viscosity, while in this work it can be relaxed since equilibrium simulations are performed.

Further, following Fan and coworkers[33], we introduced in the model a generalized weighting function (GWF^D) as

$$w_\alpha(r_{ij}) = \left(1 - \frac{r_{ij}}{r_c^D}\right)^{s_\alpha}, \quad \alpha \in \{\|, \perp\}, \tag{7}$$

It is worth noting that the GWF^D uses the dissipative cut-off radius, r_c^D, different from r_c^C, which plays a key role in the description of the transport properties without affecting the equilibrium properties. GWF^D's exponents, $s_\alpha \in (0,1]$, play an important role in modeling of dynamic properties of a DPD fluid. We do not study the exponents separately, and consider $s_\| = s_\perp = s$ for simplicity and thus, $w_\|(r_{ij}) = w_\perp(r_{ij}) = w(r_{ij})$. The standard weighting function (SWF), commonly used, is a particular case of the GWF^D in which $s = 1$ and $r_c^D = r_c^C = r_c$.

B. Time integration scheme

The EoM are integrated using VV-SSA detailed in Table I, which Nikunen et al.[34] showed to be superior with respect to several other schemes for a number of different indicators. Our previous study showed clear advantages of the VV-SSA for the solution of the extended DPD model (see Sec. II A), proven to be essential in the description of real liquids transport properties[18,19]. We found that the VV-SSA eliminates the integrator-induced artifacts and performs better in the simulation of fluids with high Schmidt numbers. Recently, Shardlow-like splitting algorithms have been further applied in DPD with various fixed conditions. In particular, the VV-SSA was shown to be

an essential improvement for practical applications of the constant-energy DPD simulations[35,36].

The VV-SSA factorizes the integration process such that the conservative forces are calculated separately from the dissipative and random terms, and the stochastic integration of the dissipative and random forces is performed prior to the deterministic integration of the conservative force. In a typical SSA formulation, both types of differential equations are integrated via the VV algorithm[37]. However, the specific choice of the VV algorithm is not a requirement. Rather, the separated stochastic and deterministic dynamics components may be solved by using any traditional MD numerical integration scheme. First based upon time-splitting, the VV-SSA decomposes the EoM into (i) differential equations that correspond to the deterministic dynamics, and (ii) elementary stochastic differential equations that correspond to the stochastic dynamics. Second based upon operator splitting, the particle stochastic dynamics are updated in a pairwise manner that conserves linear momentum[35,36].

TABLE I. Outline of the VV-SSA integration scheme to update momentum and position of each i-bead ($\mathbf{p}_i^s \to \mathbf{p}_i^{s+1}; \mathbf{r}_i^s \to \mathbf{r}_i^{s+1}$) (see text for acronym).

1. *Stochastic Integration: For all $i-j$ pairs of particles*
   a. $\mathbf{p}_i^{s+1/4} \leftarrow \mathbf{p}_i^s; \mathbf{F}_{ij}^D(\mathbf{r}_{ij}^s, \mathbf{v}_{ij}^s); \mathbf{F}_{ij}^R(\mathbf{r}_{ij}^s)$
   b. $\mathbf{p}_j^{s+1/4} \leftarrow \mathbf{p}_j^s; \mathbf{F}_{ij}^D(\mathbf{r}_{ij}^s, \mathbf{v}_{ij}^s); \mathbf{F}_{ij}^R(\mathbf{r}_{ij}^s)$
   c. $\mathbf{v}_{ij}^{s+1/4} \leftarrow \frac{\mathbf{p}_i^{s+1/4}}{m_i} - \frac{\mathbf{p}_j^{s+1/4}}{m_j}$
   d. $\mathbf{p}_i^{s+2/4} \leftarrow \mathbf{p}_i^{s+1/4}; \mathbf{F}_{ij}^D(\mathbf{r}_{ij}^s, \mathbf{v}_{ij}^{s+1/4}); \mathbf{F}_{ij}^R(\mathbf{r}_{ij}^s)$
   e. $\mathbf{p}_j^{s+2/4} \leftarrow \mathbf{p}_j^{s+1/4}; \mathbf{F}_{ij}^D(\mathbf{r}_{ij}^s, \mathbf{v}_{ij}^{s+1/4}); \mathbf{F}_{ij}^R(\mathbf{r}_{ij}^s)$
2. *Deterministic integration* #1: For $i = 1,....,N$
   a. $\mathbf{p}_i^{s+3/4} \leftarrow \mathbf{p}_i^{s+2/4} + \frac{\Delta t}{2}\mathbf{f}_i^C(\mathbf{r}^s)$
   b. $\mathbf{r}_i^{s+1} \leftarrow \mathbf{r}_i^s + \Delta t \frac{\mathbf{p}_i^{s+3/4}}{m_i}$
3. *Conservative Force Calculation:* $\left\{\mathbf{f}_i^C(\mathbf{r}^{s+1})\right\}_{i=1}^N$, where $\mathbf{f}_i^C = \sum_{j\neq i}\mathbf{F}_{ij}^C$
4. *Deterministic integration* #2: For $i = 1,....,N$
   $\mathbf{p}_i^{s+1} \leftarrow \mathbf{p}_i^{s+3/4} + \frac{\Delta t}{2}\mathbf{f}_i^C(\mathbf{r}^{s+1})$

C. Evaluation of transport coefficients in DPD

Macroscopic transport coefficients can be calculated in DPD using numerical techniques developed for atomistic simulations. Viscosity can be measured by equilibrium and non-equilibrium

methods[38]. Non-equilibrium methods are relatively straightforward to implement and they do not suffer of statistical uncertainty. However, the simulation setup can be intricate and it is specific for the transport property investigated. Non-equilibrium simulations can reproduce the experimental setup where external gradients are established, giving rise to conjugate fluxes or conversely, fluxes are imposed which result in a conjugate gradients.

In contrast, equilibrium methods such as Green-Kubo (GK) and Einstein-Helfand approaches rely on the measurement of the decay of the spontaneous thermal fluctuations of the corresponding physical property, and they do not require any specific simulation setup. Therefore, a single equilibrium simulation with periodic boundary conditions can provide a plethora of transport coefficients for different properties as commonly found in open-source MD codes. Moreover, the equilibrium methods in self-assembled systems allow the estimation of viscosity in equilibrium without altering their equilibrium self-assembled microstructures.

In this work, the GK approach[39,40] is used, which allows to calculate the viscosity by numerically integrating the stress autocorrelation function (SACF) as:

$$\eta = \frac{V}{k_B T} \int_0^{+\infty} \left\langle \Pi_{\alpha\beta}(t_0) \Pi_{\alpha\beta}(t_0 + t) \right\rangle dt, \quad (\alpha \neq \beta), \tag{8}$$

where V is the system volume and $\Pi_{\alpha\beta}$ are the off-diagonal components of the stress tensor.

Alternative GK formulas were derived independently in literature[38,41,42]. The alternative GK formula for η are obtained by splitting the stress tensor $\mathbf{\Pi}$ into conservative, dissipative, and random force contributions as[42]

$$\begin{aligned} \Pi_{zx} &= \frac{1}{V} \sum_i \left(\frac{p_i^z p_i^x}{m_i} + \sum_{j<i} z_{ij} f_{ij}^{x,C} \right) + \frac{1}{V} \sum_{i,j<i} z_{ij} f_{ij}^{x,D} + \frac{1}{V} \sum_{i,j<i} z_{ij} f_{ij}^{x,R} \\ &= \Pi_{zx}^C + \Pi_{zx}^D + \Pi_{zx}^R \end{aligned} \tag{9}$$

and pre-averaging correlations due to the random force contribution[41]. This leads to the alternative GK formula for η

$$\eta = \eta_\infty + \eta^{CC} + \eta^{CD} + \eta^{DC} + \eta^{DD} + \eta^{res}, \tag{10}$$

where (with A, B representing the composition of force components C and D)

$$\eta^{AB} = \frac{V}{k_B T}\int_0^\infty \left\langle \Pi_{zx}^{A}(t)\Pi_{zx}^{B}(0)\right\rangle dt,$$
$$\eta^{res} = \frac{V}{k_B T}\int_0^\infty \left\langle \left(\Pi_{zx}^{C}(t)+\Pi_{zx}^{D}(t)\right)\Pi_{zx}^{R}(0)\right\rangle dt,$$

and

$$\eta_\infty = \frac{V}{k_B T}\left\langle \left(\Pi_{zx}^{R}\right)^2\right\rangle \frac{\Delta t}{2}.$$

It is worth mentioning that Eq. (10) is the same as the formula by Ernst-Brito[38,41,42], i.e.,

$$\eta = \eta_\infty + \eta^{CC} - \eta^{CD} + \eta^{DC} - \eta^{DD}, \tag{11}$$

which was also obtained by the splitting of $\mathbf{\Pi}$ and evaluating all contributions of correlations due to the random contribution analytically.

In our previous works[19,21], we developed an automated method for the viscosity calculation, AMTP_DPD, which allows us to evaluate the viscosity from DPD (equilibrium) simulations with a controlled precision. The AMTP_DPD method employs the standard GK formula (8), and is outlined in the Supporting Information. In the AMTP_DPD method, we used the standard GK formula (8) rather than the alternative GK formulas (10) or (11) for practical reasons. The "full" stress tensor, containing the kinetic, and the conservative and non-conservative force contributions, is a standard output of simulation packages such as LAMMPS[28]. Outputting separately the kinetic, and the conservative and non-conservative force contributions of the stress tensor would require a non-trivial modification of the LAMMPS code with a possible additional CPU overhead. It should be also noted that for isotropic systems, the convergence of viscosity calculations can be improved by including equilibrium fluctuations of diagonal components of the stress tensor[43]. In this case, the GK formula is applied to the symmetrized traceless portion of the stress tensor with appropriate weight factors for diagonal and off-diagonal elements. More details about the AMTP_DPD method are provided in the Supporting Information and in our previous publication[21]. The AMTP_DPD code is available from the GitHub repository: https://github.com/mulmopro/AMTP_DPD.

Eqs. (10) and (11) indicate that both the conservative and non-conservative forces determine the viscosity in DPD simulations. To analyze relative magnitude of the conservative and non-

conservative contributions to η, we evaluated kinetic and conservative parts of η, η^{CC}, and subtracted it from η, leading to $\eta - \eta^{CC}$, which primarily stems from the non-conservative forces. In addition, $\eta - \eta^{CC}$ allows a comparison with theoretical predictions found in the literature.

Finally, the self-diffusion coefficient, $\mathscr{D}$, is evaluated by the Einstein relationship[44], where the self-diffusion coefficient is proportional to the mean-squared displacement (MSD) of the beads:

$$\mathscr{D} = \lim_{t \to +\infty} \frac{\left\langle [\mathbf{r}(t_0 + t) - \mathbf{r}(t_0)]^2 \right\rangle}{6t}, \tag{12}$$

$\langle . \rangle$ denotes an ensemble average.

III. COMPUTATIONAL DETAILS

All simulations were performed by using the AMTP_DPD method[21], which defines a computational protocol to compute transport properties (viscosity and diffusivity) from DPD equilibrium simulations. It uses the open-source software LAMMPS[28]. DPD simulations make use of the newly implemented `dpdext/fdt pair_style` that allow the solution of the equation of motion for the extended DPD model described in II with the VV-SSA integration scheme discussed in II. The necessary source code can be accessed via the following link: `https://github.com/mulmopro/LAMMPS-DPD-EXT`. DPD simulations are setup via a script file in which all the input parameters and the instructions for the calculations are collected. The developed algorithm bases the entire procedure of management and submission of simulations by means of the automatic generation of these files.

A system of $N = 10,125$ identical beads with $m_i = m = 1$ was simulated in a cubic box of length equal to 15 with periodic boundary conditions in all directions. The number density was set to $\rho = 3$. The temperature T varies within the liquid water range, i.e., from 278.15 K (5°C) to 363.15 K (90°C). To carry out isothermal DPD simulations across different temperatures, it was useful to introduce a temperature scale[45]. The temperature of reference $T_{\mathrm{R}} = 298.15$ K was used to scale the temperatures T. Therefore, the simulation temperature $\theta = T/T_{\mathrm{R}}$ ranges from 0.933 to 1.22; it is equal to unity only in the particular case of $T = 278.15$ K. DPD fluid interaction parameters are setup coherently with the simulation temperature θ.

The conservative repulsive parameter, a, depends on temperature according to relationships reported and commented in the Section IV B. Regarding non-conservative interaction parameters,

$\gamma_\parallel/\sigma_\parallel$ and $\gamma_\perp/\sigma_\perp$ are assumed to be equal and denoted as γ/σ; similarly for $s_\parallel = s_\perp = s$. We set $r_c^D = 1$ since increasing r_c^D increases the number of neighbouring beads and thus computational cost. The friction coefficient γ is also kept constant and equals to 20 to properly simulate liquid-like dynamics. Several studies claimed that the standard DPD $\gamma = 4.5$ cannot accurately simulate liquid-like dynamics leading to a very low Sc number[19]. In an isothermal DPD simulation, the system is implicitly connected to a heat reservoir whose temperature corresponds to the imposed temperature. During the simulation, heat is exchanged between the heat reservoir and the system such that the average kinetic temperature of the system equals the reservoir temperature. Thus, Eq. (6) indicates that the random coefficient σ depends upon the system temperature θ. Specifically keeping γ invariant with respect to θ, the random coefficient increases with increasing θ consistently with physical expectations[45]. In contrast, the s coefficient is selected as temperature-dependent parameter, and is calibrated against experimental data, Section IV B.

IV. MODELING THE EFFECT OF TEMPERATURE

A. Temperature dependent-transport properties in DPD simulations

Viscosity and self-diffusivity are temperature-dependent output properties of a DPD simulation. These properties can assume different values depending on input model parameters. Several researchers derived theoretical expressions for dynamical properties in terms of model input parameters. Among them, it is worth mentioning the relationships obtained by Groot and Warren[7], neglecting the conservative interactions. Despite of this simplification, they are in agreement with those derived by more sophisticated approaches[46] and at the same time, they highlight the physical meaning of the different terms. In particular, the effect of temperature on the various terms is clear allowing preliminary considerations on the model capability to capture the temperature-dependence of fluid transport properties. These relationships were obtained by considering the standard DPD thermostat with the SWF. Moving a step forward in the progressive evolution of the DPD model, similar relationships were derived accounting for the substitution of the SWF with a GWF, but still within the standard DPD framework[45], where shear dissipative forces are not included. It is worth highlighting that the GWF differs from the GWF^D employed in our model, since it uses as dissipative/random cut-off radius the same of the conservative one, $r_c = r_c^C = r_c^D$. For the sake of clarity, Table II shows the differences among three dissipative/random weighting

functions mentioned in this work.

TABLE II. Main differences among the weighting functions labelled by SWF, GWF and GWF^D.

Label	Exponent	Cutoff radius
SWF	1	r_c
GWF	s	r_c
GWF^D	s	r_c^D

A re-elaboration of those expressions to highlight the effect of system temperature θ on transport properties (the kinematic viscosity $\nu = \eta/\rho$ and $\mathscr{D}$) is provided in Table III. In both derivations, the first term is directly proportional to the temperature while the second term turns to be independent from the temperature, keeping invariant the model input parameters with temperature. Thus according to theoretical predictions, the kinematic viscosity described by the standard DPD model increases with increasing temperature regardless of the dissipative weighting function employed. Fig. 1 illustrates the behavior of the transport properties calculated using the SWF and GWF reported in Table III, ranging from $\theta = 0.933$ to $\theta = 1.22$. The kinematic viscosity is almost constant with respect to the temperature showing an unrealistic behavior. In both cases, the typical decaying trend of kinematic viscosity over temperature experimentally observed with many fluids such as water, ethanol, and glycerin cannot be captured.

In this work, liquid water transport properties are used as target properties and they are reported in Table IV. The experimental data of kinematic viscosity ν and self-diffusivity $\mathscr{D}$ are taken from Refs.[26,47]. Fig. 2 clearly shows that the kinematic viscosity dependence on temperature $T = \theta \times T_{\mathrm{R}}$ is opposite with respect to both the theoretical predictions as already pointed out by other works[45].

The relationship between transport properties and model interaction parameters was investigated independently in different studies also relying on numerical investigations, but not accounting for system temperature variation, usually kept constant at ambient temperature. However, only few studies considered the temperature-dependence of fluid transport properties, but using the DPD conventional formulation, which rely on parallel dissipative and random forces only. Here instead, we employed the extended DPD model detailed in Section II A since in our previous works, we pointed out that the contribution of shear dissipative forces is crucial to ensure correct description of transport properties.

TABLE III. Re-elaboration of theoretical expressions for the transport properties from literature to highlight their relationship with system temperature θ. The expressions derived in the case of the standard DPD model including the standard dissipative quadratic weighting function[7] (SWF) are compared with the ones obtained in the case of the standard DPD model including a generalized weighting function[45] (GWF^D).

Properties	**Standard thermostat (SWF)**	**Standard thermostat (GWF)**
Viscosity, ν	$\alpha_{\mathrm{SWF}}\frac{k_B\theta}{\pi\gamma\rho r_c^3}+\beta_{\mathrm{SWF}}\pi\gamma\rho r_c^5$	$\alpha_{\mathrm{GWF}}\Upsilon(s)\frac{\mathrm{k_B}\theta}{\pi\gamma\rho r_c^3}+\frac{\beta_{\mathrm{GWF}}}{\Phi(s)}\pi\gamma\rho r_c^5$
Diffusivity, $\mathscr{D}$	$2\alpha_{\mathrm{SWF}}\frac{\mathrm{k_B}\theta}{\pi\gamma\rho r_c^3}$	$2\alpha_{\mathrm{GWF}}\Upsilon(s)\frac{k_B\theta}{\pi\gamma\rho r_c^3}$
Schmidt number, Sc	$\frac{1}{2}+\frac{\beta_{\mathrm{SWF}}}{2\alpha_{\mathrm{SWF}}}\frac{(\pi\gamma\rho r_c^4)^2}{k_B\theta}$	$\frac{1}{2}+\frac{\beta_{\mathrm{GWF}}}{2\alpha_{\mathrm{GWF}}\Phi(s)\Upsilon(s)}\frac{(\pi\gamma\rho r_c^4)^2}{k_B\theta}$

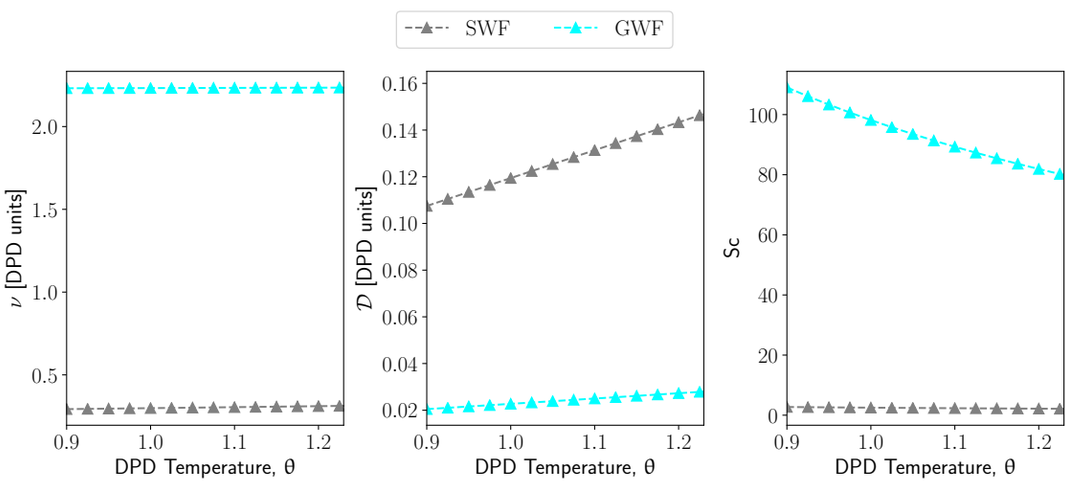

FIG. 1. Theoretically predicted behavior of the kinematic viscosity ν (left), the self-diffusivity $\mathscr{D}$ (center) and the Schmidt number Sc (right) of a DPD fluid over the system temperature θ. The SWF curves refer to standard DPD model including standard dissipative quadratic weighting function. The GWF curves refer to standard DPD model including generalized dissipative weighting function.

B. Interaction parameters

The conservative interaction parameter a is purely repulsive and its value is established via the matching of isothermal compressibility κ. The temperature dependence of the interaction parameter a was first considered by Groot and Warren (GW)[7], and recently reformulated with a

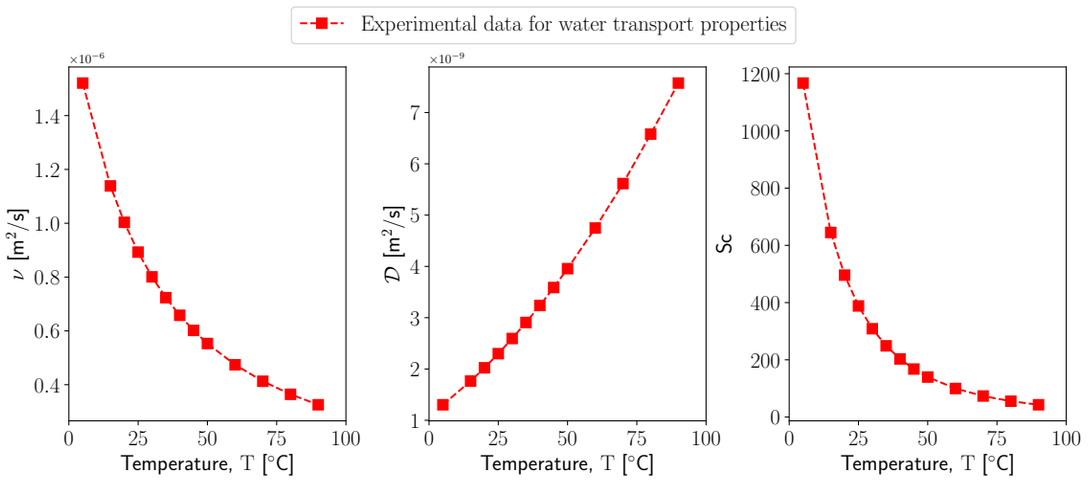

FIG. 2. Experimental behavior of the kinematic viscosity ν (left), the self-diffusivity $\mathscr{D}$ (center) and the Schmidt number Sc (right) of liquid water over temperature T.

TABLE IV. Target experimental values in real units and scaled with respect to the reference values. The reference values for the temperature T, the kinematic viscosity ν, and the self-diffusivity $\mathscr{D}$ are highlighted.

T [°C]	T [K]	θ	ν [m^2/s]	$\mathscr{D}$ [m^2/s]	ν/ν_R	$\mathscr{D}/\mathscr{D}_R$	Sc
5	278.15	0.933	1.520×10^{-6}	1.303×10^{-9}	1.703	0.5668	1167.24
15	288.15	0.966	1.138×10^{-6}	1.765×10^{-9}	1.275	0.7677	645.11
20	293.15	0.983	1.000×10^{-6}	2.023×10^{-9}	1.120	0.8799	459.99
25	298.15	1	8.926×10^{-7}	2.299×10^{-9}	1	1	388.28
30	303.15	1.02	8.007×10^{-7}	2.594×10^{-9}	0.8970	1.128	308.68
35	308.15	1.03	7.234×10^{-7}	2.907×10^{-9}	0.8104	1.264	248.86
40	313.15	1.05	6.578×10^{-7}	3.238×10^{-9}	0.7369	1.408	203.16
45	318.15	1.07	6.016×10^{-7}	3.588×10^{-9}	0.6740	1.561	167.69
50	323.15	1.08	5.531×10^{-7}	3.956×10^{-9}	0.6197	1.721	139.82
60	333.15	1.12	4.740×10^{-7}	4.748×10^{-9}	0.5310	2.065	99.83
70	343.15	1.15	4.127×10^{-7}	5.615×10^{-9}	0.4624	2.442	73.50
80	353.15	1.18	3.643×10^{-7}	6.578×10^{-9}	0.4081	2.861	55.39
90	363.15	1.22	3.254×10^{-7}	7.574×10^{-9}	0.3646	3.294	42.97

generalized approach[16]. The latter allows to include both the simulation temperature θ and the temperature-dependent compressibility κ in the evaluation of the repulsive parameter as follows:

$$a = \frac{\kappa^{-1} - k_B\theta}{2\alpha\rho}, \tag{13}$$

where α is a constant. There has been a controversy in the literature whether to take into account the level of CGing (e.g., the number of water molecules per bead) when relating the repulsive parameter to the compressibility. As shown by Füchslin et al.[48], this issue can be avoided if both the repulsive parameter and the cut-off radius are properly scaled by the level of CGing.

In many previous works, the compressibility was considered independent from temperature. This might be an overly crude approximation as in the case of water where the variation in κ is about 10% between 0°C and 50°C. In our approach, the dimensionless compressibility κ was considered temperature-dependent. The dimensionless bulk modulus κ^{-1} (the inverse of the dimensionless compressibility) depends on temperature according to the following relationship:

$$\kappa^{-1} = \kappa_{\mathrm{T}}^{-1} \frac{(r_c^C)^3}{k_{\mathrm{B}} T_{\mathrm{R}}} = \kappa_{\mathrm{T}}^{-1} \frac{\rho V_0}{k_{\mathrm{B}} T_{\mathrm{R}}}, \tag{14}$$

where κ_{T} is the water compressibility in real units [Pa^{-1}], and V_0 is the molecular volume. κ_{T} is calculated for different temperatures according to its thermodynamic definition as

$$\kappa_{\mathrm{T}}^{-1} = -\frac{1}{V} \frac{\partial V}{\partial P}\bigg|_T. \tag{15}$$

The isothermal compressibility is defined as the fractional change in the volume V that results from a change in the pressure P of the system in a process where the temperature T is constant. The thermophysical properties of water, required for the calculation, are taken from the NIST database[26]. For water at room temperature, the simulation temperature and the inverse of dimensionless compressibility are, respectively, $\theta = 1$ and $\kappa^{-1} \simeq 16$, and Eq. (13) turns into the GW form

$$a = \frac{15}{2\alpha\rho} = \frac{75}{\rho}. \tag{16}$$

where for the standard $\rho = 3$, $a = 25$. The parameter a linearly decreases with temperature as shown in Fig. 3, assuming temperature invariance of the compressibility. In Fig. 3, the different behavior of a over θ, obtained by accounting for the temperature variation of isothermal compressibility, is also reported. Moreover, Fig. 3 provides an estimate of the error on a produced by neglecting the temperature variation of the isothermal compressibility.

However, the introduction of temperature-dependent repulsive parameters is still not enough to capture temperature-dependent transport properties. In other words, the non-conservative parameters γ, r_c^D, and s capable to reproduce the viscosity η_{R} and the self-diffusivity $\mathscr{D}_{\mathrm{R}}$ of liquid water

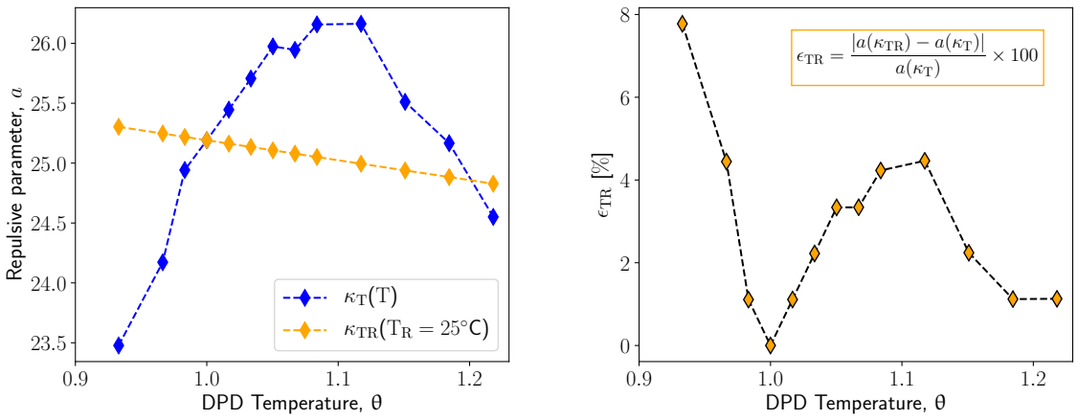

FIG. 3. Comparison between the behavior of repulsive parameters a over temperature θ obtained by assuming constant isothermal compressibility κ_{T_R} and by considering temperature-dependent isothermal compressibility values κ_T (left). Error estimates on a due to neglecting temperature variation of the isothermal compressibility (right).

at $T_R = 298.15$K fail to predict the same properties at different temperatures. This deficiency is clear from Fig. 4. Therefore to simulate a DPD fluid with realistic transport properties at different temperatures, at least one of the non-conservative interaction parameters γ, r_c^D, or s needs to be considered as temperature dependent.

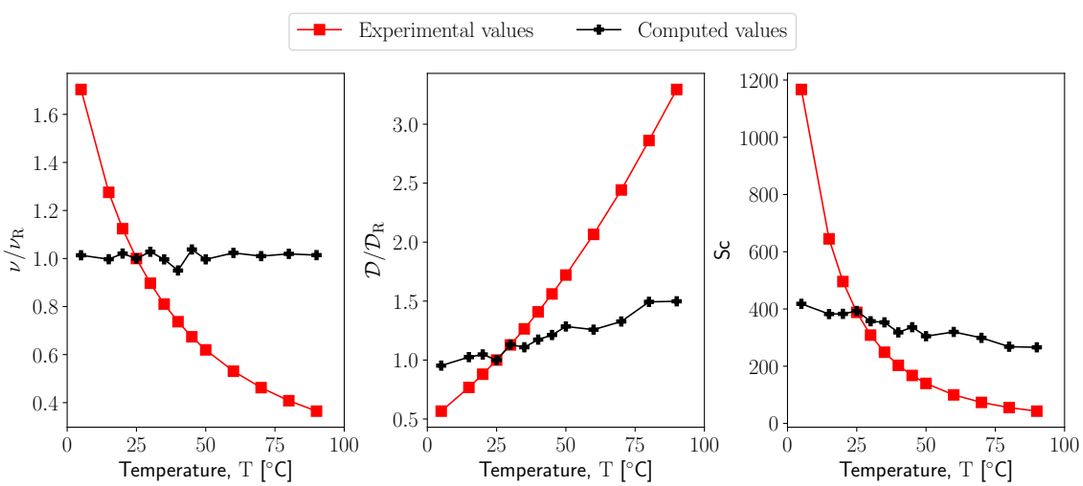

FIG. 4. Comparison of transport properties at different temperatures between experimental data and simulation results with temperature-dependent conservative and non-conservative interaction parameters. The kinematic viscosity and self-diffusivity are scaled by their reference values $\nu_R = 8.926 \times 10^{-7}\mathrm{m}^2/\mathrm{s}$ and $\mathscr{D}_R = 2.299 \times 10^{-9}\mathrm{m}^2/\mathrm{s}$ at $T_R = 298.15$K. Errors in ν and $\mathscr{D}$ are smaller than points in the viscosity plots

Our previous study[19] and other literature works detailed the effect of the parameters γ, r_c^D, and s on the transport properties. We demonstrated that the effect of γ, r_c^D, and s can be grouped

into a single quantity which measures the overall bead friction, the so-called "effective friction coefficient", defined as

$$\gamma_{\text{eff}} = 4\pi \int_0^{r_c^D} \gamma w(r_{ij})\, g(r_{ij}) r^2 dr_{ij}, \tag{17}$$

where $g(r_{ij})$ is the radial distribution function (RDF). We pointed out that fluids characterized by the same γ_{eff} have the same transport properties. In particular, there is a certain value of γ_{eff} associated to realistic transport properties of liquid water at room temperature.

According to our previous findings[19,21] to simulate liquid water at higher temperatures, the value of γ_{eff} has to be reduced to decrease the viscosity and increase the self-diffusivity consistently with experimental data. This effect can be obtained by increasing s or decreasing γ and/or decreasing r_c^D. In fact, the r_c^D acts on the number of neighbouring beads decreasing the number of the dissipative interactions. Instead, the values of γ and s modulate the strength of the dissipative interactions. The smaller γ and the higher s yield to weaker dissipative interactions, resulting in a lower viscosity and higher self-diffusivity. Similar considerations can be reached for lower temperatures. To obtain higher viscosity and smaller diffusivity, higher γ and r_c^D values are required as well as smaller s values. The definition of the dissipative coefficient γ as a function of temperature leads to physical inconsistency as already explained, e.g., in Ref.[45]. In fact, since γ and σ are related via the FDT, the reduction of γ means that hotter systems have smaller thermal fluctuations and vice versa for colder systems, which is contrary to the correct physics expectations. The value of γ is fixed for the simulations performed at different temperatures. In this way, the σ depends on θ consistently with physical expectations as described in Section III. Instead, the r_c^D and s parameters can be theoretically considered as temperature dependent.

However, in this work the r_c^D is maintained equal to r_c^C to keep the computational cost of the simulations as low as possible. This choice is feasible since the range of Sc numbers explored by liquid water (from 5°C to 90°C) is rather wide and can be covered by acting on one parameter only. Therefore for each temperature investigated within the liquid temperatures range, the s was calibrated to reproduce the Sc number consistently with experimental data. This methodology led to the derivation of an expression describing the s dependence on the simulation temperature θ presented in Section IV.

It is worth mentioning a possible scaling of DPD parameters with a coarse-graining level, Φ. In this work, we consider Füchslin et al.'s scaling approach which in reduced units, it keeps the DPD parameters and in turn, the system properties invariant under Φ. Specifically: $N' = N/\Phi$,

$m_i' = \Phi m_i$, $a' = \Phi^{2/3} a$, $r_c^{C\prime} = \Phi^{1/3} r_c^C$, $\gamma' = \Phi^{2/3}\gamma$, $\sigma' = \Phi^{5/6}\sigma$, $t' = \Phi^{1/3} t$, and the unit of energy, $(k_\mathrm{B}T)' = \Phi(k_\mathrm{B}T)$, where primed variables correspond to Φ. Two notes are appropriate for Füchslin et al.'s scaling approach.

First, Füchslin et al. pointed out that the validity of their approach does not necessarily hold for the study of dynamical properties, and they demonstrated it on the scaling of diffusion. They showed that the relative particle motions are unaffected by scaling in the reduced unit systems, i.e., trajectories are numerically equal. On the one hand, this leads to the numerical equivalence of the measured diffusion coefficients but on the other hand, the fact that the diffusion coefficient scales like length squared over time causes an apparent problem. It seemingly implies that relative fluctuations of the reduced diffusion coefficient over the reduced length stay constant instead of vanishing with increasing Φ, which is a consequence of Füchslin et al.'s CGing. It brings a general question to what extent the trajectories of DPD particles can be understood as representing actual transport processes.[49] Several authors[50,51] resolve the calibration problem by treating the natural time unit as undetermined and instead obtain the physical time scale from calibrating diffusion coefficients measured in simulation to physical values.[51]

Second, Füchslin et al.'s scalings of the non-conservative coefficients, γ and σ, was suggested for the DPD method with the parallel non-conservative forces and the SWF. In this work, we consider the parallel and perpendicular non-conservative forces and the GWF$^\mathrm{D}$. This may require examining validity of the scalings of the γ and σ coefficients, and determining a scaling of the GWF$^\mathrm{D}$ coefficients, s. A possible route towards the scaling of these GWF$^\mathrm{D}$ coefficients may involve considering the effective friction coefficient, Eq. (17), invariant under Φ in reduced units. However, this is beyond the scope of this work.

C. Results and discussion

To ensure the reliability and correctness of the simulation insights, checking the behavior of the system kinetic temperature during simulation runs is essential for each temperature investigated. In particular, the average kinetic temperature, $\theta_\mathrm{avg} = \langle \mathscr{T}_\mathrm{kin} \rangle$, should be equal to the imposed temperature θ. The standard deviation of θ can be considered acceptable if lower than 2% according to the criteria proposed by Groot and Warren[7]. Table V shows that θ_avgs are around the average value with standard deviations lower than 2%, i.e., the time integration scheme employed properly guarantees the kinetic temperature control during the simulation runs at each temperature investigated.

The performance of the VV-SSA to solve the isothermal extended DPD EoM for the evaluation of transport properties was already proven to be superior to other schemes at $\theta = 1$ in our previous work[21]. Table V provides evidence that the VV-SSA performs excellently when θs vary in the range from 0.933 to 1.22. The kinetic temperature control is important to preserve the meaningfulness of the physical insights provided from each isothermal simulation performed. Otherwise, unphysical drifts of the kinetic temperature would lead to uncontrolled spatial correlations among particles and to significant errors in the simulated static and dynamical properties.

TABLE V. Targeted system temperature θ, the average kinetic temperature θ_{avg} and associated standard deviation θ_{std} for each temperature T investigated.

T [°C]	θ	θ_{avg}	θ_{std} [%]
5	0.933	0.932	0.7
15	0.966	0.966	0.7
20	0.983	0.983	0.7
25	1	0.999	0.8
30	1.020	1.020	0.8
35	1.030	1.029	0.8
40	1.050	1.049	0.8
45	1.070	1.070	0.8
50	1.080	1.088	0.8
60	1.120	1.119	0.9
70	1.150	1.149	0.9
80	1.180	0.180	0.9
90	1.220	1.220	0.9

Due to the DPD soft interactions and rather large simulation boxes typically employed in DPD simulations, the finite size error of $\mathscr{D}$ due to periodic boundary conditions, in contrast to molecular dynamics simulations, can be expected to be rather small. Nevertheless, we performed DPD simulations at $\theta = 1$, and varied box lengths of the cubic simulation box, L, from 12 to 40. We then plotted evaluated values of the self-diffusion coefficient, $\mathscr{D}^{\text{PBC}}$, as a function of $1/L$ as shown in Fig. 2 of the Supporting Information. Analogously to MD simulations[52], we represented $\mathscr{D}^{\text{PBC}}$ as

$$\mathscr{D}^{\text{PBC}} = \mathscr{D}^{0} - \frac{k_{\text{B}} T \xi}{6\pi\eta L} \tag{18}$$

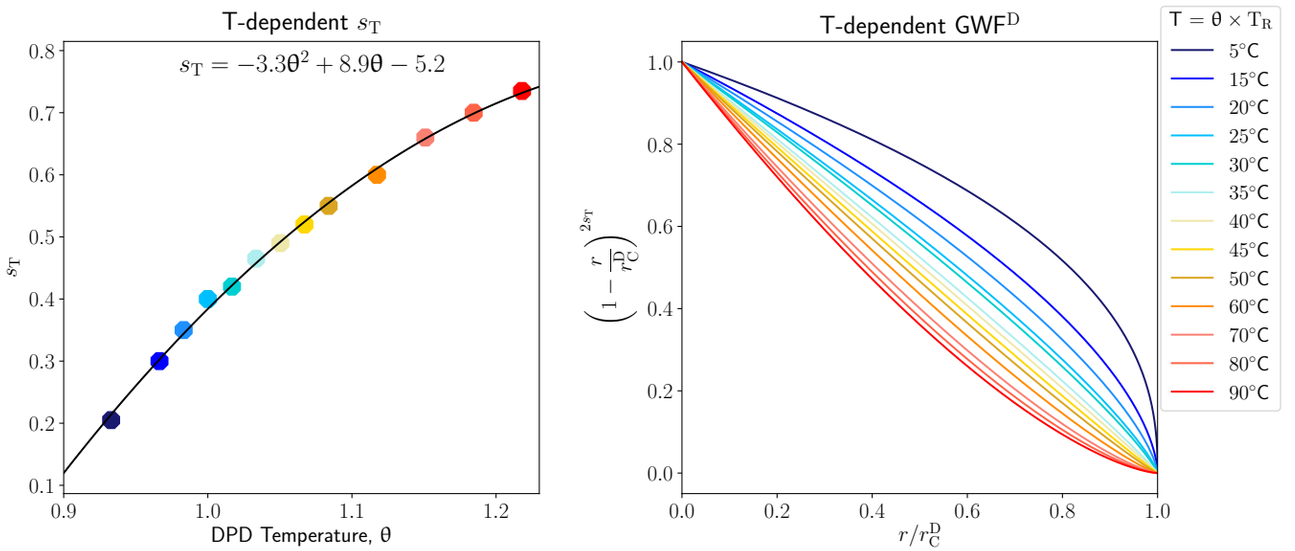

FIG. 5. The s power coefficient as a function of temperature θ which provides the correct Sc number of liquid water at different real temperatures $T = T_R \times \theta$. The fitting of those data gives s as a function of θ (left). Dissipative weighting functions at different temperatures $T = T_R \times \theta$ (right).

where $\mathscr{D}^0$ is the "true" self-diffusion coefficient, and $\xi = 1.855157$. Note that $\xi = 1.855157$ is smaller than $\xi = 2.837297$ relevant for MD simulations[52], and in turn, $\mathscr{D}^{\mathrm{PBC}}$ vs $1/L$ is less steep in DPD simulations than that in MD simulations. We then use Eq. (18) to evaluate values of $\mathscr{D}^0$ at different temperatures. We found that differences between values of $\mathscr{D}^{\mathrm{PBC}}$ and $\mathscr{D}^0$ are up to 2%, which has no or negligible effect on the adjustment of the non-conservative DPD parameters, see the Supporting Information for details. The values of $\mathscr{D}^{\mathrm{PBC}}$ were employed below.

For each temperature investigated, the s power coefficient was calibrated to capture the correct Sc number of liquid water. The Sc number measured by DPD is compared with the experimental Sc for each temperature investigated in the range from $T = 5°\mathrm{C}$ to $T = 90°\mathrm{C}$, which corresponds to the DPD temperature range from $\theta = 0.933$ to $\theta = 1.22$. Table VI reports the experimental Sc, $\mathrm{Sc}_{\mathrm{exp}}$, and the DPD Sc, $\mathrm{Sc}_{\mathrm{DPD}}$, for each temperature T together with the relative error. The level of acceptability of the error was fixed to be lower than 5% a priori. The s values capable to satisfy this matching condition for each temperature are also reported in Table VI, and are plotted in Fig. 5.

The s power coefficient modulates the strength of non-conservative interactions within the volume defined by r_c^D. To get transport properties behavior consistently with experiments, the s parameter needs to incorporate the system temperature variation. Fig. 5 shows how different values of s lead to different behavior of the GWF^D at different temperatures. Room temperature water

transport properties are properly reproduced with $s = 0.40$. It is clear that higher/smaller temperatures require smaller/higher values of s to accurately describe momentum and mass transport. Since smaller s yields stronger non-conservative interactions, resulting in turn into a higher Sc and vice versa, the obtained s trend over temperature was expected. The fitting of those data gives s as a function of θ according to the following expression:

$$s_{\mathrm{T}} = -3.3\theta^2 + 8.9\theta - 5.2, \tag{19}$$

Eq. (19) allows to reproduce liquid water transport properties consistently with experimental data.

TABLE VI. Values of the non-conservative parameter, s, providing an excellent match between the experimental Schmidt number, $\mathrm{Sc}_{\mathrm{exp}}$, and the DPD Schmidt number, $\mathrm{Sc}_{\mathrm{DPD}}$, for each temperature, T, as evident from the relative error $\varepsilon_{\mathrm{Sc}}$.

T [°C]	θ	$\mathrm{Sc}_{\mathrm{exp}}$	$\mathrm{Sc}_{\mathrm{DPD}}$	$\varepsilon_{\mathrm{Sc}}$[%]	s
5	0.933	1167.24	1125.19	3.6	0.205
15	0.966	645.11	654.04	1.3	0.300
20	0.983	459.99	504.19	1.6	0.350
25	1.00	388.28	392.91	1.1	0.400
30	1.02	308.68	317.33	2.7	0.420
35	1.03	248.86	249.92	0.6	0.465
40	1.05	203.16	211.98	4.3	0.490
45	1.07	167.69	173.35	3.2	0.520
50	1.08	139.82	142.95	2.1	0.550
60	1.12	99.83	101.35	1.4	0.600
70	1.15	73.50	73.74	0.3	0.660
80	1.18	55.39	55.52	0.2	0.700
90	1.22	42.97	53.44	1.0	0.735

Fig. 6 exhibits the comparison of the temperature-dependent kinematic viscosity, self-diffusivity and Sc number between the DPD simulations and experiments. The extended DPD model is able to properly capture temperature variations of both the viscosity and self-diffusivity over temperature in the range from $T = 5$°C to $T = 90$°C. This outcome remarks the importance of properly modeling non-conservative interactions to correctly describe real fluids transport properties. The use of the extended DPD model in which the s parameter is reconsidered as a temperature-dependent

parameter s_T is crucial in the achievement of the realistic decaying trend of the kinematic viscosity over temperature.

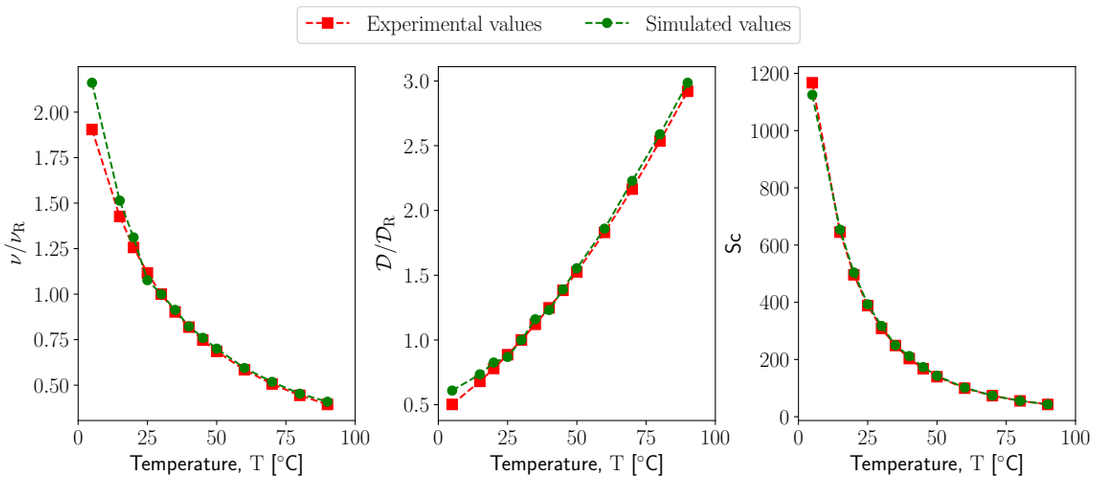

FIG. 6. Comparison of the transport properties at different temperatures between experimental data and the results of DPD simulations with the temperature-dependent conservative interaction parameter a and the temperature-dependent non-conservative interaction parameter s. The kinematic viscosity and diffusivity are scaled by their reference values at ν_R and $\mathscr{D}_R$ at $T_R = 25°C$.

In fact, the left subplot of Fig. 7 clearly highlights that the main contribution to the kinematic viscosity ν is given by $\nu - \nu^{CC}$, where $\nu^{CC} = \eta^{CC}/\rho$, cf. Eq. (10); similarly for $\nu - \nu^{CC}$. The latter ignores the contribution to the viscosity that arises from $\Pi^C_{\alpha\beta}$, which gathers the contribution to the stress tensor given by the kinetic and conservative forces, see Eq. (9). The $\nu - \nu^{CC}$ represents the contribution to the viscosity that arises primarily from non-conservative interactions. It is quantitatively most of the viscosity and it is more sensitive than ν^{CC} to temperature variation. This outcome is the proof that the capability to properly capture the viscosity dependence on temperature basically depends on the definition of the temperature-dependent non-conservative parameter s_T.

Moreover, the evaluation of $\nu - \nu^{CC}$ allows comparison with theoretical predictions since they are derived by neglecting the conservative forces, see Section IV A. The comparison is still approximate since the theoretical expressions also do not take into account the cross terms ν^{CD} and ν^{DC} of Eq. (10), but it is significant for the investigation carried out in this work. The right plot of Fig. 7 compares our viscosity values $\nu - \nu^{CC}$ at different temperatures and the ones predicted by two different theoretical expressions available in literature and discussed in the Section IV A. The ν^{SWF} theoretical expression is obtained considering the standard DPD thermostat with the SWF;

the s parameter is fixed to one for all fluids. Instead, ν^{GWF} theoretical expression is obtained assuming a standard DPD thermostat with the GWF^D. In this case, s can assume different values depending on type of fluids simulated.

In the right subplot of Fig. 7, ν^{GWF} is computed assuming $s = 0.4$. However in both expressions, s as an input parameter is independent from the system temperature. Although both theoretical predictions can give only a rough estimate of the viscosity since they are derived via a simplified approach, the behavior of the curves makes clear that the effect of temperature on viscosity cannot be described by the DPD models assumed in their derivation. In fact, ν^{SWF} are much smaller than the realistic ones due to the absence of shear dissipation, whose inclusion has been proved to be essential to describe liquid-like dynamics. Moreover, they are almost constant with respect to the system temperature. The ν^{GWF} values are higher than the ν^{SWF} ones as expected, since the s parameter is smaller and it yields stronger non-conservative interactions. However, the ν^{GWF} viscosities due to the introduction of a smaller s are still almost constant and independent of the system temperature. Instead, our $\nu - \nu^{CC}$s are high enough to provide realistic Sc numbers for liquid water and they also vary with temperature consistently with the expected experimental trend.

First, this result indicates that the extended DPD model employed and based on the transverse DPD thermostat with the GWF^D, provides the quantitative match between simulated and experimental transport properties. Second, it demonstrates that the methodology based on modeling the s parameter as a function of the system temperatures is successful to capture temperature-dependent transport properties.

Fig. 8 reports the values of the effective friction coefficient γ_{eff} measured at different temperatures. As expected, it decreases as the temperature increases. The simulation γ_{eff}s are fitted to

$$\gamma_{\mathrm{eff}} = 102.9\theta^{-3} - 269.1\theta^{-1.5} + 236.7\theta^{-1} - 69.5. \tag{20}$$

The main contribution to γ_{eff}'s variation with temperatures comes from non-conservative interactions since the contribution from the RDF integration is almost constant. The RDFs do not vary significantly with the system temperature as shown in the left subplot of Fig. 8 where the RDFs at different temperatures almost overlapped.

To assess the model goodness-of-fit, the coefficient of determination (R-squared) and the normalized root-mean-squared error (NRMSE) are reported in Table VII for all the fitting relations

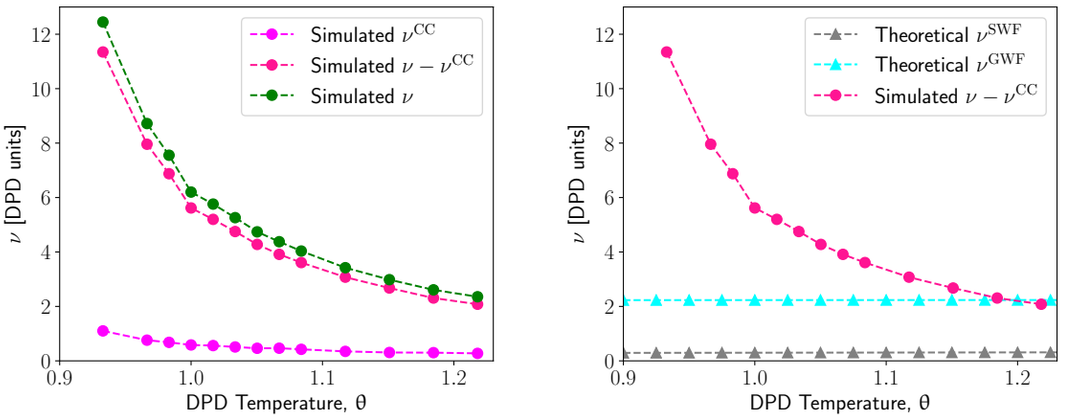

FIG. 7. Kinematic viscosity ν obtained from DPD simulations at different temperatures θ splitted into ν^{CC} and $\nu - \nu^{CC}$ contributions (left). Comparison between $\nu - \nu^{CC}$ simulated and the theoretical predictions of Fig. 1 (right).

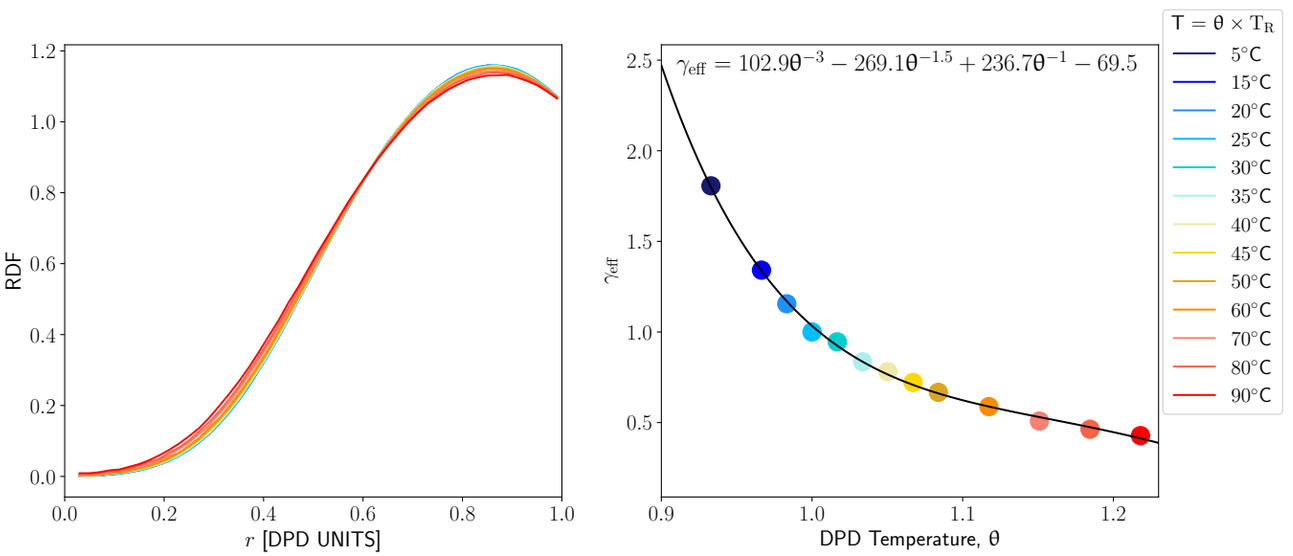

FIG. 8. Radial distribution function for each temperature investigated $T = T_R \times \theta$ (left). Effective friction coefficient γ_{eff} obtained at different temperatures (right).

derived in this study. All the fitting relationships recovered present goodness-of-fit measures with the same order of magnitude.

V. CONCLUSIONS

This work investigated the use of the extended dissipative particle dynamics (DPD) model, numerically solved with the Shardlow-splitting-algorithm-based integration scheme, as a compu-

TABLE VII. Goodness-of-fit measures from the fitting of the s values and the effective friction coefficient values γ_{eff}.

Fitted quantity	R^2	$NRMSE$
s_T	0.9980	0.0128
γ_{eff}	0.9983	0.0112

tational tool to predict temperature-dependent transport properties at the mesoscale following a top-down coarse-graining. The transport properties calculation from equilibrium simulations was performed using an in-house developed automated and reliable method, available online.

A temperature-dependent form of the extended DPD model, where both conservative and non-conservative interaction parameters incorporate the system temperature variation, was proposed. In particular, liquid water was used as model system in this work. Experimental data of transport properties[26,27] from 5°C to 90°C were used as target values to develop and validate the model. The extended DPD model allows the simulation of water dynamics across different temperatures within the whole liquid range consistently with experimental data of viscosity and self-diffusivity. Although the model was developed and validated against transport properties of liquid water, it can also be used as a first rough estimation for the non-conservative parameters of other liquids.

The temperature-dependent form of the extended DPD model of this work can be further extended to multicomponent systems or systems with chain-like molecules. For the conservative interaction parameters, which are based on Groot-Warren's DPD parameterization[7], the temperature-dependent compressibility can be used to determine like repulsive parameters, a_{ii}, at various temperatures. Unlike repulsive parameters, a_{ij}, can be determined from a linear relationship between a_{ij} and the Flory-Huggins interaction parameter, which is inherently temperature-dependent. Alternatively for systems with chemically distinctly different beads or local density variations, Kacar et al.'s DPD parameterization can be used, which explicitly involves a temperature dependence[53,54]. Parameters of non-conservative forces can be adjusted analogously as in this work to the viscosity and mutual self-diffusion coefficients. However, adjustment will involve different $itype - jtype$ pairs, e.g., 1-1, 1-2, and 2-2 type-pairs for a binary system, and may become rather complex and demanding. Such the adjustment may benefit from machine learning methods.

The outcomes of this work would also be useful for future developments of non-isothermal

DPD models. In fact, the energy conserving DPD (DPDe) is slowly growing as a powerful tool in capturing temperature-induced mesoscopic phenomena, but it requires the definition of temperature-dependent interactions. The incorporation of a temperature-dependent conservative force-field was presented in different studies and it was shown to be capable of predicting the behavior of equilibrium properties induced by a thermal gradient. Instead on the other hand, the incorporation of temperature-dependent dissipative and random forces, such as those proposed in this work, is less straightforward. It requires further theoretical development to properly modify the DPDe framework. However, this extension is interesting and crucial to exploit DPDe as a computational tool to simulate at the mesoscale also the transport properties behavior induced by a thermal gradient.

VI. SUPPLEMENTARY MATERIAL

Readers are encouraged to consult the Supplementary Information material for a comprehensive description of the AMTP_DPD method utilized for the computation of transport properties. The Supplementary Information material also contains detailed numerical information regarding the reliability assessment of viscosity and diffusivity calculations.

ACKNOWLEDGMENTS

Computational resources were provided by HPC@POLITO. We acknowledge the CINECA award under the ISCRA initiative, for the availability of high-performance computing resources and support. The financial support from ICSC (Centro Nazionale di Ricerca in High Performance Computing, Big Data and Quantum Computing, funded by European Union - NextGenerationEU) is also gratefully acknowledged. This study was carried out within the "Non-equilibrium self-assembly of structured fluids: a multi-scale engineering problem" project – funded by European Union – Next Generation EU within the PRIN 2022 program (D.D. 104 - 02/02/2022 Ministero dell'Università e della Ricerca). This manuscript reflects only the authors' views and opinions and the Ministry cannot be considered responsible for them.

AUTHOR CONTRIBUTIONS

Nunzia Lauriello: Conceptualization (equal); Data curation (lead); Formal analysis (equal); Investigation (equal); Methodology (equal); Software (lead); Writing – original draft (lead). **Martin Lísal**: Conceptualization (equal); Formal analysis (equal); Investigation (equal); Methodology (equal); Writing - review & editing (lead). **Gianluca Boccardo**: Conceptualization (equal), Supervision (equal); Writing - review & editing (equal). **Daniele Marchisio**: Conceptualization (equal), Funding acquisition (lead); Project administration (lead); Supervision (equal); Writing - review & editing (equal). **Antonio Buffo**: Conceptualization (equal), Supervision (equal); Writing - review & editing (equal).

DATA AVAILABILITY

The code used for the simulations can be found online at https://github.com/mulmopro/AMTP_DPD. The necessary LAMMPS source code can be accessed through this link: https://github.com/mulmopro/LAMMPS-DPD-EXT.

REFERENCES

[1]R. Larson, *The Structure and Rheology of Complex Fluids* (Oxford University Press, 1999).

[2]Y. R. Sliozberg, J. W. Andzelm, J. K. Brennan, M. R. Vanlandingham, V. Pryamitsyn, and V. Ganesan, Journal of Polymer Science Part B: Polymer Physics **48**, 15 (2010).

[3]M. Ferrari, J.-W. Handgraaf, G. Boccardo, A. Buffo, M. Vanni, and D. L. Marchisio, Physics of Fluids **34**, 021903 (2022).

[4]F. De Roma, D. Marchisio, G. Boccardo, M. Bouaifi, and A. Buffo, Physics of Fluids **36**, 023119 (2024).

[5]K. Šindelka and M. Lísal, Molecular Physics **119**, e1857863 (2021).

[6]K. Procházka, Z. Limpouchová, M. Štěpánek, K. Šindelka, and M. Lísal, Polymers **14**, 35160394 (2022).

[7]R. D. Groot and P. B. Warren, The Journal of Chemical Physics **107**, 4423 (1997).

[8]P. Español and P. B. Warren, The Journal of Chemical Physics **146**, 150901 (2017).

[9]P. J. Hoogerbrugge and J. M. V. A. Koelman, Europhysics Letters (EPL) **19**, 155 (1992).

[10]P. Español, Physical Review E **57**, 2930 (1998).

[11]M. B. Liu, G. R. Liu, L. W. Zhou, and J. Z. Chang, Archives of Computational Methods in Engineering **22**, 529 (2015).

[12]K. P. Santo and A. V. Neimark, Advances in Colloid and Interface Science **298**, 102545 (2021).

[13]J. B. Avalos, M. Lísal, J. P. Larentzos, A. D. Mackie, and J. K. Brennan, Physical Chemistry Chemical Physics **21**, 24891 (2019).

[14]J. B. Avalos, M. Lísal, J. P. Larentzos, A. D. Mackie, J. K. Brennan, and J. K. Brennan, Physical Review E **103**, 062128 (2021).

[15]M. Lísal, J. P. Larentzos, J. B. Avalos, A. D. Mackie, and J. K. Brennan, Journal of Chemical Theory and Computation **18**, 2503 (2022).

[16]P. Vanya, J. Sharman, and J. A. Elliott, The Journal of Chemical Physics **150**, 064101 (2019).

[17]E. Mayoral and A. G. Goicochea, The Journal of Chemical Physics **138**, 094703 (2013).

[18]S. Izvekov and B. M. Rice, Physical Chemistry Chemical Physics **17**, 10795 (2015).

[19]N. Lauriello, J. Kondracki, A. Buffo, G. Boccardo, M. Bouaifi, M. Lísal, and D. Marchisio, Physics of Fluids **33**, 073106 (2021).

[20]C. Junghans, M. Praprotnik, and K. Kremer, Soft Matter **4**, 156 (2008).

[21]N. Lauriello, G. Boccardo, D. Marchisio, M. Lísal, and A. Buffo, Computer Physics Communications **291**, 108843 (2023).

[22]S. Trément, B. Schnell, L. Petitjean, M. Couty, and B. Rousseau, The Journal of Chemical Physics **140**, 134113 (2014).

[23]S. Izvekov and B. M. Rice, The Journal of Chemical Physics **140**, 104104 (2014).

[24]H. Mori, Progress of Theoretical Physics **33**, 423–455 (1965).

[25]R. Zwanzig, The Journal of Chemical Physics **33**, 1338 (1965).

[26]E. W. Lemmon, M. O. McLinden, and D. G. Friend, in *NIST Chemistry Webbook, NIST Standard reference database*, Vol. 69, edited by P. J. Linstrom and W. G. Mallard (National Institute of Standards and Technology, Gaithersburg MD, 20899, USA, 1998).

[27]M. Holz, S. R. Heil, and A. Sacco, Physical Chemistry Chemical Physics **2**, 4740 (2023).

[28]A. P. Thompson, H. M. Aktulga, R. Berger, D. S. Bolintineanu, W. M. Brown, P. S. Crozier, P. J. in 't Veld, A. Kohlmeyer, S. G. Moore, T. D. Nguyen, R. Shan, M. J. Stevens, J. Tranchida, C. Trott, and S. J. Plimpton, Computer Physics Communication **271**, 108171 (2022).

[29]P. Español and P. Warren, Europhysics Letters (EPL) **30**, 191 (1995).

[30]R. C. Krafnick and A. E. García, The Journal of Chemical Physics **143**, 243106 (2015).

[31]C.-C. Fu, P. M. Kulkarni, M. S. Shell, and L. G. Leal, The Journal of Chemical Physics **139**, 094107 (2013).

[32]W. Pan, I. V. Pivkin, and G. E. Karniadakis, EPL (Europhysics Letters) **84**, 10012 (2008).

[33]X. Fan, N. Phan-Thien, S. Chen, X. Wu, and T. Y. Ng, Physics of Fluids **18**, 063102 (2006).

[34]P. Nikunen, M. Karttunen, and I. Vattulainen, Computer Physics Communications **153**, 407 (2022).

[35]M. Lísal, J. K. Brennan, and J. Bonet Avalos, AIP Publishing **135**, 1 (2011).

[36]J. P. Larentzos, J. K. Brennan, J. D. Moore, M. Lísal, and W. D. Mattson, Computer Physics Communications **185**, 1987 (2014).

[37]T. Shardlow, Journal on Scientific Computing **24**, 1267 (2003).

[38]G. Jung and F. Schmid, The Journal of Chemical Physics **144**, 204104 (2016).

[39]M. S. Green, The Journal of Chemical Physics **22**, 398 (1954).

[40]R. Kubo, Journal of the Physical Society of Japan **12**, 570 (1957).

[41]M. H. Ernst and R. Brito, Europhysics Letters **73**, 183 (2006).

[42]D. C. Malaspina, M. Lísal, J. P. Larentzos, J. K. Brennan, A. D. Mackie, and J. Bonet Avalos, Physical Chemistry Chemical Physics **26**, 1328 (2024).

[43]D. Bedrov, G. D. Smith, and T. D. Sewell, J. Chem. Phys. **112**, 7203 (2000).

[44]J.-P. Hansen and I. R. McDonald, *Theory of Simple Liquids* (Academic Press, Amsterdam, Netherlands, 2013).

[45]Z. Li, Y.-H. Tang, H. Lei, B. Caswell, and G. E. Karniadakis, Journal of Computational Physics **265**, 113 (2014).

[46]C. A. Marsh, G. Backx, and M. H. Ernst, Physical Review E **56**, 1676 (1997).

[47]B. Leimkuhler and X. Shang, Journal of Computational Physics **280**, 72 (2015).

[48]R. M. Füchslin, H. Fellermann, A. Eriksson, and H.-J. Ziock, The Journal of Chemical Physics **130**, 214102 (2009).

[49]R. Groot, *Novel Methods in Soft Matter Simulations*, Lecture Notes in Physics, Vol. 640 (Springer Berlin, Heidelberg, 2004).

[50]A. F. Jakobsen, O. G. Mouritsen, and M. Weiss, Journal of Physics: Condensed Matter **17** (2005).

[51]R. Groot and K. Rabone, Biophysical Journal **81**, 725 (2001).

[52]I.-C. Yeh and G. Hummer, The Journal of Physical Chemistry B **108**, 15873 (2004).

[53]G. Kacar, E. A. J. F. Peters, and G. de With, Europhys. Lett. **102**, 40009 (2013).

[54]G. Kacar, E. A. J. F. Peters, and G. de With, Soft Matter **9**, 5785 (2013).